

# A Three-Dimensional Tight-Binding Model and Magnetic Instability of $\text{KFe}_2\text{Se}_2$

Da-Yong Liu<sup>1</sup>, Ya-Min Quan<sup>1</sup>, Zhi Zeng<sup>1</sup>, Liang-Jian Zou<sup>1,a</sup>

<sup>1</sup> *Key Laboratory of Materials Physics,  
Institute of Solid State Physics,  
Chinese Academy of Sciences,  
P. O. Box 1129, Hefei 230031,  
People's Republic of China*

(Dated: Mar 20, 2011)

## Abstract

For a newly discovered iron-based high  $T_c$  superconducting parent material  $\text{KFe}_2\text{Se}_2$ , we present an effective three-dimensional five-orbital tight-binding model by fitting the band structures. The three  $t_{2g}$ -symmetry orbitals of the five Fe 3d orbitals mainly contribute to the electron-like Fermi surface, in agreement with recent angle-resolved photoemission spectroscopy experiments. To understand the groundstate magnetic structure, the two- and three-dimensional dynamical spin susceptibilities within the random phase approximation are investigated. It obviously shows a sharp peak at wave vector  $\mathbf{Q} \sim (\pi, \pi)$ , indicating the magnetic instability of *Néel*-type antiferromagnetic rather than  $(\pi/2, \pi/2)$ -type antiferromagnetic ordering. While along  $c$  axis, it exhibits a ferromagnetic coupling between the nearest neighboring FeSe layers.

PACS numbers: 74.70.Xa, 74.20.Pq, 71.10.-w

## I. INTRODUCTION

Since the discovery of the iron-based superconductor has been reported [1], a series of superconducting compounds were found, such as 1111 phase (*e.g.* LaOFeAs [1]), 122 phase (*e.g.* BaFe<sub>2</sub>As<sub>2</sub> [2]), 111 phase (*e.g.* NaFeAs [3]), and 11 phase (*e.g.* FeSe [4], FeTe [5]). Recently a new superconductor member KFe<sub>2</sub>Se<sub>2</sub> with  $T_c$  above 30 K (K<sub>0.8</sub>Fe<sub>2</sub>Se<sub>2</sub>) [6] has been reported, and attracted considerable interests for its unique insulator and large magnetic moment properties, quite different from other iron-based superconducting materials for its parent material KFe<sub>2</sub>Se<sub>2</sub> is iso-structural to BaFe<sub>2</sub>As<sub>2</sub>, but chemically close to FeSe.

The space group of KFe<sub>2</sub>Se<sub>2</sub> at room temperature is I4/mmm (No. 139) [6]. Its crystal structure is composed of edge-sharing FeSe<sub>4</sub> tetrahedra separated by K cations, as shown schematically in Fig. 1.

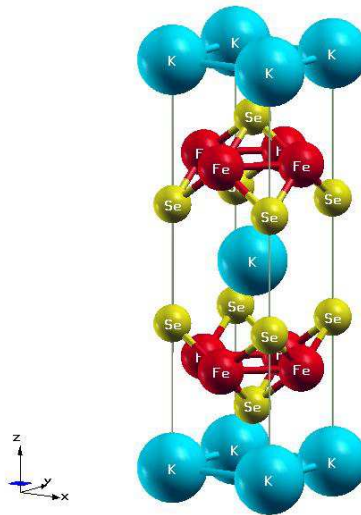


FIG. 1. Crystal structure of KFe<sub>2</sub>Se<sub>2</sub> with a tetragonal unit cell (space group I4/mmm), the axes X and Y are along the diagonal Fe-Se direction. The crystal structure parameters are adopted from Ref. [6].

In KFe<sub>2</sub>Se<sub>2</sub>, there are formally 6.5 electrons per Fe, rather than 6 in other iron-based parent materials. Thus it is regarded as an electron over-doped 11 system. As a consequence, the hole-like Fermi surface pockets possessed in other iron-based materials disappear, and only the electron-like Fermi surface pockets were observed in recent angle-resolved photoemission spectroscopy (ARPES) experiments [7, 8] and predicted in recent band structure calculations [9, 10]. Thus, the Fermi surface nesting, which is widely suggested to be the origin of the striped-antiferromagnetic (AFM) ( $\pi, 0$ ) spin density wave (SDW) in FeAs-based materials, together with the inter-band

scattering of the Fermi surface, which is widely believed to be important for the superconducting pairing in FeAs-based superconductor, is absent in  $\text{KFe}_2\text{Se}_2$  compound. And the strongly three-dimensional characteristic of the Fermi surface is also found in  $\text{KFe}_2\text{Se}_2$ .

Early experiment showed that both  $\text{TlFe}_2\text{Se}_2$  [11] and  $\text{TlFeS}_2$  [12] are AFM compounds. In a recent experiment, the high-temperature magnetic susceptibility decreases with the decrease of the temperature, indicating that the Fe spins interact with each other through the AFM coupling [13]. However, the magnetic ordering structure is still an debating issue, as addressed in what follows. The local density approximation (LDA) calculations suggested that  $\text{KFe}_2\text{Se}_2$  is a striped AFM order, same to the 1111 and 122 phases of the FeAs-based materials [10], while some other authors [9] thought it to be bi-collinear AFM with  $(\pi/2, \pi/2)$  wave-vector, similar to FeTe [5]. On the other hand, for Fe-deficient materials,  $\text{K}_{0.8}\text{Fe}_{1.6}\text{Se}_2$  *etc.*, the block checkerboard AFM order is observed experimentally, in which its origin is attributed to the ordered Fe vacancy [14, 15]. Moreover, the density function theory (DFT) calculations suggested the  $\text{TlFe}_2\text{Se}_2$  is a checkerboard AFM order [16]. These discrepant results indicate that further investigations on the magnetic ordering structure are urgent for understanding the unique properties in  $\text{AFe}_2\text{Se}_2$  (A=K, Tl, or Cs) compounds.

In this paper, we have made our efforts to resolve this debate. Based on our LDA calculated results, we propose a three-dimensional five-orbital model for  $\text{KFe}_2\text{Se}_2$ , and show its dynamical spin susceptibility diverges at wavevector  $\mathbf{Q}=(\pi, \pi, 0)$ , suggesting C-type AFM magnetic instability, *i.e.* a *Néel*-type AFM coupling in the *ab*-plane and a weak ferromagnetic coupling along the *c*-axis. This paper is organized as follows: the LDA band structure, Fermi surface and a five-orbital tight-binding model fitting to the band structures are presented in *Sec. II*; the dynamical spin susceptibility obtained in the random phase approximation (RPA) is shown in *Sec. III*; the last section is devoted to the remarks and summary.

## II. TIGHT-BINDING FITTING OF THE BAND STRUCTURES

The parent material  $\text{KFe}_2\text{Se}_2$  has a tetragonal layered structure with Fe atoms forming a square lattice in the high temperature phase. The experimental lattice parameters are  $a=b=3.9136\text{\AA}$  and  $c=14.0367\text{\AA}$  at room temperature [6]. There are two Fe atoms per unit cell, where each Fe is tetrahedrally coordinated by Se. We have performed a band structure calculation of  $\text{KFe}_2\text{Se}_2$  using the full-potential linearized augmented plane-wave plus local orbitals (FP-LAPW+lo) scheme implemented in the WIEN2K package [17]. The band structure calculations for other iron-based

materials showed that the electronic structure is sensitive to a small structural distortion. Thus, in order to compare with the experiments, we adopted the experimental structural data [6]. The density of states (DOS), the Fermi surface and the band structures within the LDA are displayed in Fig. 2, Fig. 3 and Fig. 4, respectively. From the DOS in Fig. 2, it is obviously found that

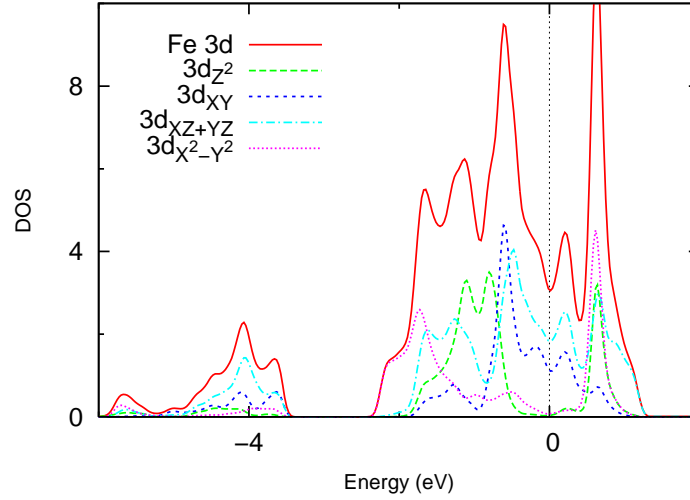


FIG. 2. The total and partial density of states of Fe obtained by LDA.

this compound is a metal in high-temperature phase, and the Fermi surface is mainly contributed by three orbitals,  $XZ$ ,  $YZ$  and  $XY$ . Meanwhile the  $d_{3z^2-R^2}$  and  $d_{x^2-y^2}$  bands mainly distribute from  $-2.6$  eV to  $E_F$ , with a little contribution to the Fermi surface, suggesting that the  $\text{KFe}_2\text{Se}_2$  is essentially a five-band system, similar to other iron pnictides. The Fermi surface of  $\text{KFe}_2\text{Se}_2$  is plotted

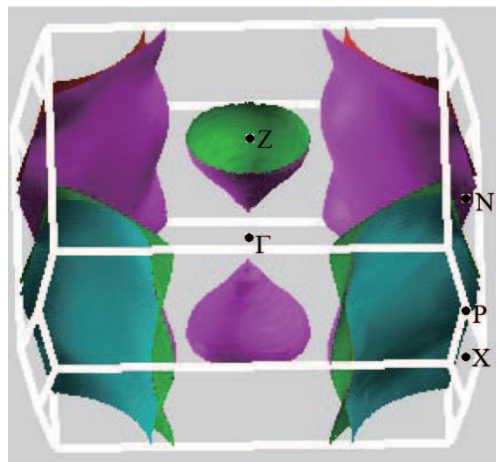


FIG. 3. Fermi surface obtained within the LDA for parent material  $\text{KFe}_2\text{Se}_2$  in folded Brillouin zone.

in Fig. 3, displaying a three-dimensional characteristic with four electron-like Fermi surface pock-

ets at corner, and two electron-like Fermi surface pockets along  $\Gamma$ - $Z$  direction in folded Brillouin zone. The hole-like Fermi surface pockets at  $\Gamma$  are absent, and only the electron-like Fermi surface pockets are presented, which is in agreement with the recent ARPES experiments [7, 8] and band structure calculations [9, 10].

The band structures of the undoped  $\text{KFe}_2\text{Se}_2$  in high-temperature phase are shown in Fig. 4. To implement our further study, we fit the band structures with a five-orbital tight-binding model. Note that the orientation of the coordinate system is chosen so that Fe-Fe bonds are directed along the  $x$  and  $y$  axes, in which  $x$  and  $y$  axes are rotated by 45 degrees from the  $X$ - $Y$  axes, where the  $X$  and  $Y$  axes, along the diagonal Fe-Se direction, refer to the original unit cell. The tight-binding Hamiltonian for the five-orbital model is described as,

$$H_0 = \sum_{\substack{i,j \\ \alpha,\beta,\sigma}} t_{ij}^{\alpha\beta} C_{i\alpha\sigma}^\dagger C_{j\beta\sigma} - \mu \sum_{i\alpha\sigma} n_{i\alpha\sigma} \quad (1)$$

where  $C_{i\alpha\sigma}^\dagger$  creates an electron on site  $i$  with orbital  $\alpha$  and spin  $\sigma$ ,  $t_{ij}^{\alpha\beta}$  is the hopping integral between the  $i$  site with  $\alpha$  orbital and the  $j$  site with  $\beta$  orbital, and  $\mu$  is the chemical potential determined by the electron filling. In the momentum space the Hamiltonian  $H_0$  is expressed as

$$H_0 = \sum_{k,\alpha,\beta,\sigma} (\epsilon_\alpha \delta_{\alpha\beta} + T^{\alpha\beta}(\mathbf{k})) C_{k\alpha\sigma}^\dagger C_{k\beta\sigma}, \quad (2)$$

where  $T^{\alpha\beta}(\mathbf{k})$  is the kinetic energy term, and  $\epsilon_\alpha$  denotes the on-site energy of the  $\alpha$  orbital. The five-orbital tight-binding fit of the 10 Fe-3d bands obtained by the density functional theory band structure is displayed in Fig. 4.

The model parameters for the five-orbital tight-binding fitting of the  $\text{KFe}_2\text{Se}_2$  band structure are listed in the following. The on-site energies measured from the Fermi energy for the five orbitals are  $(\epsilon_1, \epsilon_2, \epsilon_3, \epsilon_4, \epsilon_5) = (-346.7, -346.7, -437.4, -176.4, -927.9)$ , respectively, in units of meV. Here orbital indices (1,2,3,4,5) indicate the  $d_{xz}$ ,  $d_{yz}$ ,  $d_{x^2-y^2}$  ( $d_{XY}$ ),  $d_{xy}$  ( $d_{X^2-Y^2}$ ), and  $d_{3z^2-r^2}$  components, respectively. Similar to  $\text{BaFe}_2\text{As}_2$  [18], the hopping integrals along each direction are

$$\begin{aligned} T^{11/22} &= 2t_{x/y}^{11} \cos k_x + 2t_{y/x}^{11} \cos k_y + 4t_{xy}^{11} \cos k_x \cos k_y \\ &\quad \pm 2t_{xx}^{11} (\cos 2k_x - \cos 2k_y) + 4t_{xy/xy}^{11} \cos 2k_x \cos k_y \\ &\quad + 4t_{yy/xy}^{11} \cos 2k_y \cos k_x + 4t_{xxy}^{11} \cos 2k_x \cos 2k_y \\ &\quad + 4t_{xz}^{11} (\cos k_x + \cos k_y) \cos k_z \pm 4t_{xxz}^{11} (\cos 2k_x - \cos 2k_y) \cos(k_z), \end{aligned}$$

$$T^{33} = 2t_x^{33} (\cos k_x + \cos k_y) + 4t_{xy}^{33} \cos k_x \cos k_y + 2t_{xx}^{33} (\cos 2k_x + \cos 2k_y),$$

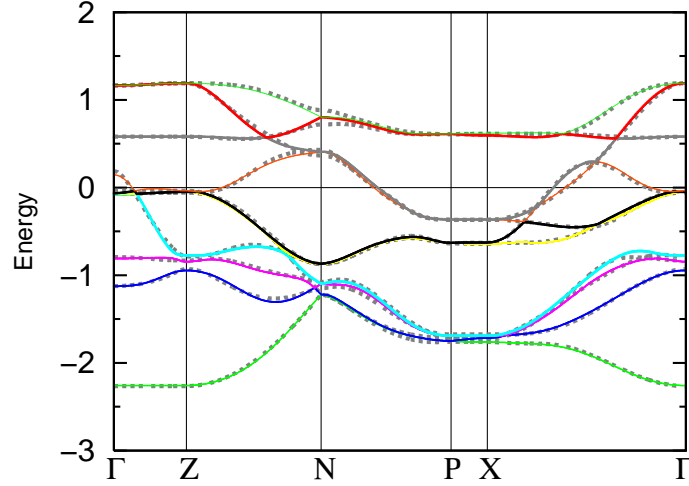


FIG. 4. The band structures of the Fe-3d orbitals obtained by the full-potential linearized-augmented-plane-wave (LAPW) and its five-orbital tight-binding fitting. The dot lines are the present local-density approximation results, the solid lines are the fitting results. The energies are measured from the Fermi energy  $E_F=0.409$  eV.

$$\begin{aligned}
T^{44} = & 2t_x^{44}(\cos k_x + \cos k_y) + 4t_{xy}^{44}\cos k_x\cos k_y + 2t_{xx}^{44}(\cos 2k_x + \cos 2k_y) \\
& + 4t_{xxy}^{44}(\cos 2k_x\cos k_y + \cos 2k_y\cos k_x) + 4t_{xxyy}^{44}\cos 2k_x\cos 2k_y \\
& + 2t_z^{44}\cos k_z + 4t_{xz}^{44}(\cos k_x + \cos k_y)\cos k_z + 8t_{xyz}^{44}\cos k_x\cos k_y\cos k_z,
\end{aligned}$$

$$\begin{aligned}
T^{55} = & 2t_x^{55}(\cos k_x + \cos k_y) + 4t_{xy}^{55}\cos k_x\cos k_y + 2t_{xx}^{55}(\cos 2k_x + \cos 2k_y) \\
& + 4t_{xxy}^{55}(\cos 2k_x\cos k_y + \cos 2k_y\cos k_x) + 4t_{xxyy}^{55}\cos 2k_x\cos 2k_y \\
& + 2t_z^{55}\cos k_z + 4t_{xz}^{55}(\cos k_x + \cos k_y)\cos k_z,
\end{aligned}$$

$$\begin{aligned}
T^{12} = & 4t_{xy}^{12}\sin k_x\sin k_y + 4t_{xxy}^{12}(\sin 2k_x\sin k_y + \sin 2k_y\sin k_x) \\
& + 4t_{xxyy}^{12}\sin 2k_x\sin 2k_y + 8t_{xyz}^{12}\sin k_x\sin k_y\cos k_z,
\end{aligned}$$

$$\begin{aligned}
T^{13/23} = & 2it_x^{13}\sin k_{y/x} + 4it_{xy}^{13}\cos k_{x/y}\sin k_{y/x} \\
& - 4it_{xxy}^{13}(\sin 2k_{y/x}\cos k_{x/y} - \cos 2k_{x/y}\sin k_{y/x}),
\end{aligned}$$

$$\begin{aligned}
T^{14/24} = & \pm 2it_x^{13}\sin k_{x/y} \pm 4it_{xy}^{14}\cos k_{y/x}\sin k_{x/y} \\
& \pm 4it_{xxy}^{14}\cos k_{y/x}\sin 2k_{x/y} \pm 4it_{xzy}^{14}\sin k_{x/y}\cos k_z \\
& - 4t_{xz}^{24}\sin k_{x/y}\sin k_z \pm 8it_{xyz}^{14}\cos k_{y/x}\sin k_{x/y}\cos k_z \\
& \pm 8it_{xxyz}^{14}\sin 2k_{x/y}\cos k_{y/x}\cos k_z - 8t_{xxyz}^{24}\sin 2k_{x/y}\cos k_{y/x}\sin k_z,
\end{aligned}$$

$$T^{15/25} = \pm 2it_x^{15} \text{sink}_{y/x} \mp 4it_{xy}^{15} \text{cos}k_{x/y} \text{sink}_{y/x} \\ \mp 8it_{xyz}^{15} \text{cos}k_{x/y} \text{sink}_{y/x} \text{cos}k_z,$$

$$T^{34} = 4t_{xxy}^{34} (\text{sin}2k_y \text{sink}_x - \text{sin}2k_x \text{sink}_y),$$

$$T^{35} = 2t_x^{35} (\text{cos}k_x - \text{cos}k_y) + 4t_{xxy}^{35} (\text{cos}2k_x \text{cos}k_y - \text{cos}2k_y \text{cos}k_x).$$

$$T^{45} = 4t_{xy}^{45} \text{sink}_x \text{sink}_y + 4t_{xxy}^{45} \text{sin}2k_x \text{sin}2k_y \\ + 2it_z^{45} \text{sink}_z + 4it_{xz}^{45} (\text{cos}k_x + \text{cos}k_y) \text{sink}_z,$$

The intra-orbital and inter-orbital hopping parameters up to fifth neighbors of the five-orbital model for the fit of the band structure are shown in Table I.

TABLE I. The intra-orbital  $t_i^{\alpha\alpha}$  and inter-orbital  $t_i^{\alpha\beta}$  hopping parameters up to fifth neighbors of the five orbital tight-binding model through fitting the band structures. All the parameters are in units of meV.

$t_i^{\alpha\alpha}$	i=x	i=y	i=xy	i=xx	i=xxy	i=xyy	i=xyxy	i=z	i=xz	i=xxz	i=xyz
$\alpha=1$	-15.6	-236.7	198.2	10.5	-42.2	13.1	27.9		-1.7	12.2	
$\alpha=3$	355.0		-77.4	-22.7							
$\alpha=4$	-3.4		54.5	-28.0	-17.0		-32.3	66.0	30.1		15.3
$\alpha=5$	66.1			6.5	-17.8		-2.7	18.0	-6.8		
$t_i^{\alpha\beta}$	i=x	i=xy	i=xxy	i=xyxy	i=z	i=xz	i=xyz	i=xyzy			
$\alpha\beta=12$		41.3	0.7	21.3			45.9				
$\alpha\beta=13$	-302.7	122.5	22.6								
$\alpha\beta=14$	-213.2	-26.2	1.7			-11.3	4.9	-10.6			
$\alpha\beta=15$	-87.3	-103.3					7.8				
$\alpha\beta=24$						-24.5		13.9			
$\alpha\beta=34$			1.7								
$\alpha\beta=35$	-293.9		-6.9								
$\alpha\beta=45$		68.0		-32.7	-65.6	7.7					

### III. DYNAMICAL SPIN SUSCEPTIBILITY

In this section we study the dynamical spin susceptibility of the five-orbital tight-binding model for  $\text{KFe}_2\text{Se}_2$ . The dynamical magnetic susceptibility is calculated for both the non-interaction case and the electron-electron interaction case within the RPA.

The orbital-dependent dynamical spin susceptibility is given by [19, 20]

$$\chi_{\alpha\gamma}(\mathbf{q}, i\omega) = \int_0^\beta d\tau e^{i\omega\tau} \langle T_\tau \mathbf{S}_\alpha(\mathbf{q}, \tau) \cdot \mathbf{S}_\gamma(-\mathbf{q}, 0) \rangle \quad (3)$$

where  $\alpha$  and  $\gamma$  label the orbital indices, and the spin operator  $\mathbf{S}_\alpha(\mathbf{q}) = \frac{1}{2} \sum_{k,mn} C_{\alpha m}^\dagger(\mathbf{k} + \mathbf{q}) \boldsymbol{\sigma}_{mn} C_{\alpha n}(\mathbf{k})$  with spin indices  $m, n$ , and  $\beta = 1/k_B T$ . The physical dynamical spin susceptibility reads  $\chi(\mathbf{q}, i\omega) = \frac{1}{2} \sum_{\alpha\gamma} \chi_{\alpha\gamma}(\mathbf{q}, i\omega)$ , with

$$\chi_{\alpha\gamma}(\mathbf{q}, i\omega) = -\frac{1}{N} \sum_{k,\mu\nu} \frac{b_\mu^\alpha(\mathbf{k}) b_\mu^{\gamma*}(\mathbf{k}) b_\nu^\gamma(\mathbf{k} + \mathbf{q}) b_\nu^{\alpha*}(\mathbf{k} + \mathbf{q})}{i\omega + E_\nu(\mathbf{k} + \mathbf{q}) - E_\mu(\mathbf{k})} [f(E_\nu(\mathbf{k} + \mathbf{q})) - f(E_\mu(\mathbf{k}))]. \quad (4)$$

Here, the matrix elements of the eigenvector  $b_\mu^\alpha(\mathbf{k}) = \langle \alpha | \boldsymbol{\mu} \mathbf{k} \rangle$  with indices connecting  $\alpha$  orbital and  $\mu$  band, are determined by the diagonalization of the tight-binding model Hamiltonian Eq. (2).

In the presence of the Coulomb interaction, in addition to the kinetic term in Eq. (2), the electronic interaction part of the multiorbital Hamiltonian reads,

$$\begin{aligned} H_I = & U \sum_{i,\alpha} n_{i\alpha\uparrow} n_{i\alpha\downarrow} + U' \sum_{\substack{i \\ \alpha \neq \beta}} n_{i\alpha\uparrow} n_{i\beta\downarrow} + (U' - J_H) \sum_{\substack{i,\sigma \\ \alpha < \beta}} n_{i\alpha\sigma} n_{i\beta\sigma} \\ & - J_H \sum_{\substack{i \\ \alpha \neq \beta}} C_{i\alpha\uparrow}^\dagger C_{i\alpha\downarrow} C_{i\beta\downarrow}^\dagger C_{i\beta\uparrow} + J_H \sum_{\substack{i \\ \alpha \neq \beta}} C_{i\alpha\uparrow}^\dagger C_{i\alpha\downarrow}^\dagger C_{i\beta\downarrow} C_{i\beta\uparrow} \end{aligned} \quad (5)$$

where  $U(U')$  denotes the intra-(inter-)orbital Coulomb repulsion interaction and  $J_H$  the Hund's rule coupling. Considering the symmetry of the system, we adopt  $U' = U - 2J_H$ . The RPA dynamical magnetic susceptibility is described as

$$\chi^{RPA}(\mathbf{q}, i\omega) = \chi_0(\mathbf{q}, i\omega) [\mathbb{I} - \Gamma \chi_0(\mathbf{q}, i\omega)]^{-1} \quad (6)$$

where  $\chi_0$  is the bare spin susceptibility defined in Eq. (4), and the nonzero components of the matrices  $\Gamma$  are given as  $(\Gamma)_{\alpha\alpha} = U$ , and  $(\Gamma)_{\alpha\neq\gamma} = J_H$ . Note that the interorbital interaction  $U'$  doesn't contribute to the RPA spin susceptibility [20].

To investigate the effect of the  $k_z$ -dependence of  $\chi(\mathbf{q}, i\omega)$ , we study the two-dimensional case with fixed  $k_z$  and  $q_z=0$ , and the three-dimensional case with integrating over  $k_z$  and fixed  $q_z$ , respectively. Fig. 5 plots the  $q$ -dependence of the real part of the bare and RPA dynamical magnetic

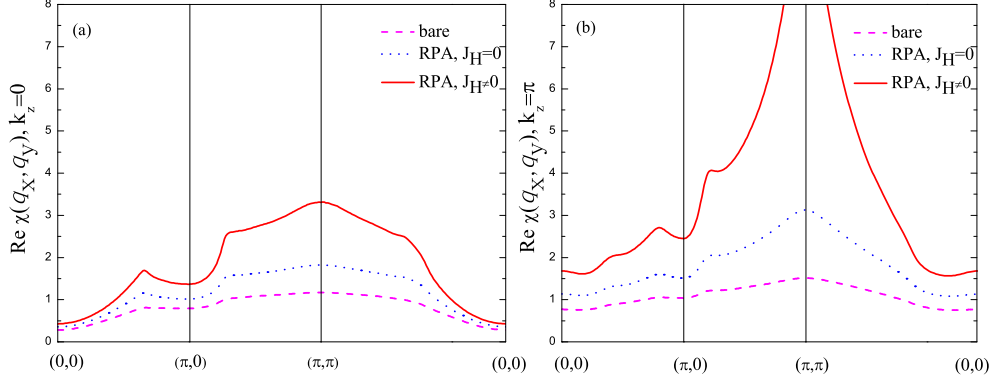


FIG. 5. Real part of the bare and RPA enhanced susceptibility along the main symmetry directions of the Fe/cell Brillouin zone for  $k_z=0$  (a),  $\pi$  (b) in the two-dimensional case ( $k_z$  is fixed and  $q_z=0$ ). Theoretical parameters  $U=0.6$  eV,  $J_H=0$ , or  $0.25U$  ( $\neq 0$ ), and  $\beta=0.02$ .

susceptibilities in the two-dimensional case for  $k_z=0$  and  $\pi$  along the main symmetry directions of the Fe/cell Brillouin zone, respectively. It is found that the bare spin susceptibility is nearly a plateau-like structure, which is almost equivalent both for  $k_z=0$  and for  $k_z=\pi$ , without obvious peak. As a comparison, the RPA dynamical spin susceptibility is considerably enhanced due to the presence of the Coulomb interaction, and a small peak appears at  $Q=(\pi, \pi)$ . Furthermore, in the presence of both Coulomb interaction and finite Hund's rule coupling,  $J_H \neq 0$ , the  $(\pi, \pi)$  susceptibility peak is greatly enhanced. Moreover, the RPA spin susceptibility of the  $k_z=\pi$  cut is obviously larger than that of the  $k_z=0$  cut. In addition to a small peak along the  $(0, 0)$ - $(\pi, 0)$  line, the largest peak appears at  $Q=(\pi, \pi)$ , indicating the magnetic instability of the *Néel*-type AFM order rather than that of the bi-collinear AFM order with  $Q=(\pi/2, \pi/2)$ , or of the striped AFM order with  $Q=(\pi, 0)$ . Similar behaviors are also seen in Fig. 6, which displays the contour of the real part of the RPA dynamical magnetic susceptibility for fixed value  $k_z=0$  (see (a) and (c)), and  $\pi$  (see (b) and (d)) in the  $q_x$ - $q_y$  plane in the two-dimensional case.

Considering the three-dimensional characteristic of Fermi surface in  $\text{KFe}_2\text{Se}_2$ , as seen in Fig. 3, we also present the  $k_z$  evolution of the magnetic susceptibility. Similar to the two-dimensional case, the three-dimensional bare and RPA dynamical susceptibilities are calculated for fixed  $q_z$  values,  $q_z=0$  or  $\pi$ . As expected, the peaks of the dynamical magnetic susceptibility are suppressed in the three-dimensional case, in comparison with the two-dimensional result. To clearly show the magnetic instability in the three-dimensional case, we displays the susceptibilities at  $U=0.7$  eV, as shown in Fig. 7. We find that the peak grows up and the divergent tendency of  $\chi(\mathbf{q})$

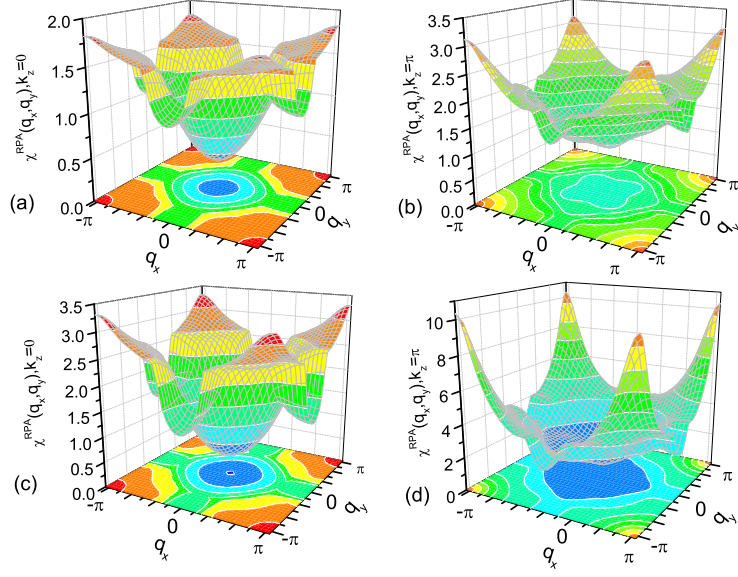


FIG. 6. Contour of the real part of the RPA dynamical magnetic susceptibility of  $k_z=0$  ((a) and (c)), and  $\pi$  ((b) and (d)) in the two-dimensional case ( $k_z$  is fixed and  $q_z=0$ ). The theoretical parameters: Coulomb interaction  $U=0.6$  eV,  $J_H=0$  ((a) and (b)), and  $0.25U$  ((c) and (d)), and  $\beta=0.02$ .

becomes strong with the increase of the electronic correlations. In realistic compound  $K_x\text{Fe}_2\text{Se}_2$ , the Coulomb interaction  $U$  is obviously larger than  $0.7$  eV, implying that the divergency of the  $\chi(\mathbf{q})$  is much stronger than the present situation shown in Fig. 7. Thus the strong divergency in the dynamical magnetic susceptibility suggests the magnetic instability or spin ordering in  $K_x\text{Fe}_2\text{Se}_2$ .

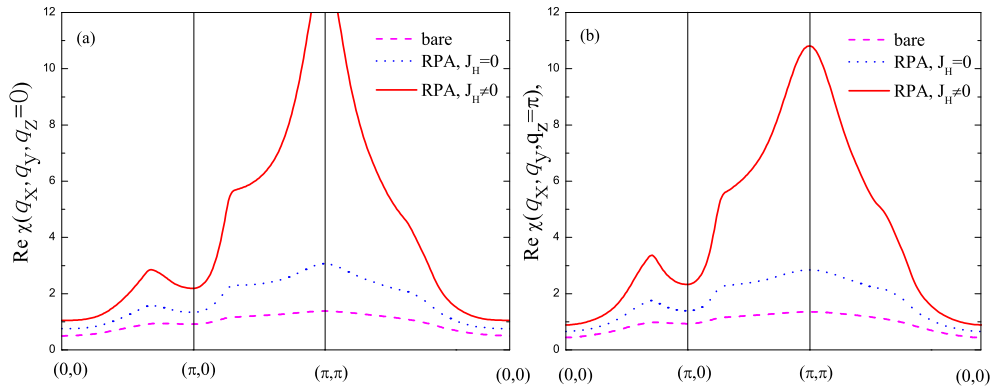


FIG. 7. Real part of the bare and RPA dynamical magnetic susceptibility along the main symmetry directions of the Fe/cell Brillouin zone for  $q_z=0$  (a),  $\pi$  (b) in the three-dimensional case. We adopt  $U=0.7$  eV,  $J_H=0$ ,  $0.25U$  ( $\neq 0$ ), and  $\beta=0.02$ .

The dynamical susceptibility in Fig. 7 shows a small peak in the  $(0, 0)$ - $(\pi, 0)$  line and a large peak around at  $(\pi, \pi)$ , similar to the two-dimensional case. The sharp peak in the spin susceptibility at  $q_z=0$  indicates a  $(\pi, \pi, 0)$  three-dimensional magnetic structure with ferromagnetic coupling between the nearest-neighbor FeSe layers in  $\text{KFe}_2\text{Se}_2$ , *i.e.* it shows a ferromagnetic coupling along the  $c$ -axis and an AFM coupling in the  $ab$ -plane (C-type AFM). Notice that the interlayer coupling is weak due to the long distance between the nearest-neighbor Fe layers along the  $c$ -axis. Other LDA calculations [9] for both  $\text{CsFe}_2\text{Se}_2$  and  $\text{KFe}_2\text{Se}_2$  also suggested a ferromagnetic coupling along  $c$  axis, in agreement with our result. However, the structures of the spin susceptibility of  $q_z=0$  and  $\pi$  remain qualitatively the same, as shown in Fig. 8.

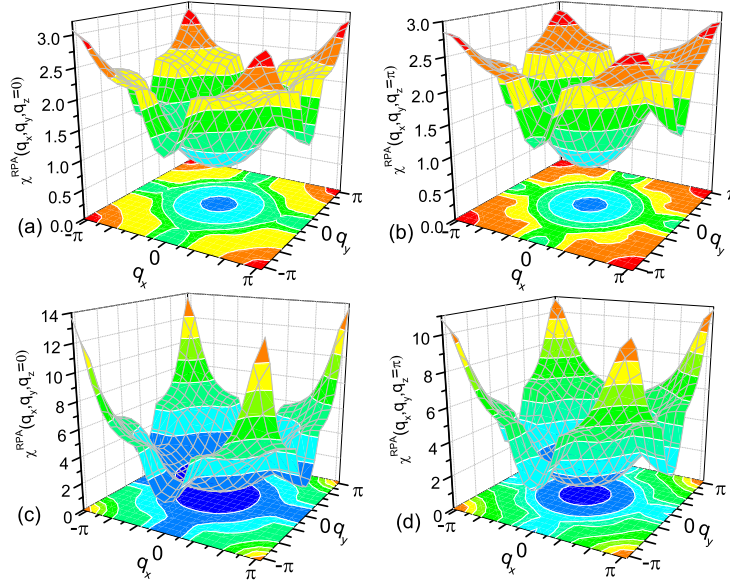


FIG. 8. Contour of the real part of the RPA dynamical magnetic susceptibility for  $q_z=0$  ((a) and (c)), and  $\pi$  ((b) and (d)) in the three-dimensional case. The Coulomb interaction  $U=0.7$  eV,  $J_H=0$  (a) and (b),  $0.25U$  (c) and (d), and  $\beta=0.02$  are adopted.

On the contrary, the first-principles electronic structure calculations suggested the striped AFM in  $\text{KFe}_2\text{Se}_2$  [10], or the bi-collinear AFM ordering in  $\text{AFe}_2\text{Se}_2$  ( $A=\text{K}, \text{Tl}, \text{or Cs}$ ) [9]. Though Zhang and Singh's *Néel*-type AFM configuration in  $\text{TlFe}_2\text{Se}_2$  [16] agrees with our results in the  $ab$ -plane, the magnetic coupling along the  $c$ -axis is different. The origin of the difference in these *ab initio* results is unknown. In our study, we deal with the electronic correlation in the framework of the RPA. Considering the fact that the FeSe-based materials with large magnetic moments may be intermediate or strong correlated systems, a proper treatment on the electronic correlation in

these FeSe-based compounds may be important for understanding its magnetic ground state.

On the other hand, it is found in the recent experiments that the ordered Fe vacancies in  $\text{K}_{0.8}\text{Fe}_{1.6}\text{Se}_2$  lead to a block checkerboard AFM order in the square Fe layers with a large magnetic moment  $3.31 \mu_B$  and  $T_N \sim 559$  K [14], then an Fe vacancy order-disorder transition occurs at  $T_S \sim 578$  K. In addition, it is also shown that the AFM order is reduced [21] with the increasing Fe content. The block checkerboard AFM order observed in the experiments of  $\text{K}_{0.8}\text{Fe}_{1.6}\text{Se}_2$  is confirmed in recent LDA calculations [22]. Meanwhile,  $\text{AFe}_{1.5}\text{Se}_2$  (A=K, Tl, Rb, or Cs) displays a A-collinear AFM by the LDA calculations [23]. Obviously, our prediction on the C-type AFM magnetic ordering in  $\text{KFe}_2\text{Se}_2$  is different from these experimental observations, showing that Fe vacancy with the lattice dynamics plays a key role in these Fe-deficient materials.

#### IV. SUMMARY

In summary, we have presented a five-orbital tight-binding model for newly found  $\text{KFe}_2\text{Se}_2$ , the energy dispersion and Fermi surface are also given. In addition, we also investigated the spin fluctuation through the multi-orbital dynamical spin susceptibility within the random phase approximation. The results demonstrate a divergent peak appears at the wavevector  $\mathbf{Q}=(\pi, \pi, 0)$ , indicating a C-type antiferromagnetic ordering in the parent compound  $\text{KFe}_2\text{Se}_2$ . Future experiment for parent materials  $\text{KFe}_2\text{Se}_2$  are expected to confirm this kind of magnetic ordering. Further theoretical studies on the dynamical magnetic susceptibility for the Fe-deficient compounds are also deserved.

#### ACKNOWLEDGMENTS

The author (D.Y.) gratefully acknowledge the help by Guo-Ren Zhang and Yan-Ling Li. This work was supported by the Natural Science Foundation of China (NSFC) No. 11047154, 11074257, and of Anhui Province No. 11040606Q56, and the Knowledge Innovation Program of the Chinese Academy of Sciences. Numerical calculations were performed at the Center for Computational Science of CASHIPS.

---

[1] Y. Kamihara, T. Watanabe, M. Hirano, and H. Hosono, *J. Am. Chem. Soc.* **130**, 3296 (2008).

- [2] Q. Huang, Y. Qiu, W. Bao, M. A. Green, J. W. Lynn, Y. C. Gasparovic, T. Wu, G. Wu, and X. H. Chen, *Phys. Rev. Lett.* **101**, 257003 (2008).
- [3] G. F. Chen, W. Z. Hu, J. L. Luo, and N. L. Wang, *Phys. Rev. Lett.* **102**, 227004 (2009).
- [4] F. C. Hsu, J. Y. Luo, K. W. Yeh, T. K. Chen, T. W. Huang, P. M. Wu, Y. C. Lee, Y. L. Huang, Y. Y. Chu, D. C. Yan, and M. K. Wu, *Proc. Natl. Acad. Sci. U.S.A.* **105**, 14262 (2008).
- [5] W. Bao, Y. Qiu, Q. Huang, M. A. Green, P. Zajdel, M. R. Fitzsimmons, M. Zhernenkov, S. Chang, M. H. Fang, B. Qian, E. K. Vehstedt, J. H. Yang, H. M. Pham, L. Spinu, and Z. Q. Mao, *Phys. Rev. Lett.* **102**, 247001 (2009).
- [6] J. G. Guo, S. F. Jin, G. Wang, S. C. Wang, K. X. Zhu, T. T. Zhou, M. He, and X. L. Chen, *Phys. Rev. B* **82**, 180520(R) (2010).
- [7] Y. Zhang, L. X. Yang, M. Xu, Z. R. Ye, F. Chen, C. He, H. C. Xu, J. Jiang, B. P. Xie, J. J. Ying, X. F. Wang, X. H. Chen, J. P. Hu, M. Matsunami, S. Kimura, and D. L. Feng, *Nature materials* **10**, 273 (2011).
- [8] T. Qian, X. P. Wang, W. C. Jin, P. Zhang, P. Richard, G. Xu, X. Dai, Z. Fang, J. G. Guo, X. L. Chen, and H. Ding, *Phys. Rev. Lett.* **106**, 187001 (2011).
- [9] X. W. Yan, M. Gao, Z. Y. Lu, and T. Xiang, arXiv: 1012.5536 (unpublished).
- [10] C. Cao and J. H. Dai, arXiv: 1012.5621 (unpublished).
- [11] L. Häggström, H. R. Verma, S. Bjarman, R. Wäppling, and R. Berger, *J. Solid State Chem.* **63**, 401 (1986).
- [12] H. Sabrowsky, M. Rosenberg, D. Welz, P. Deppe, and W. Schäfer, *J. Magn. Magn. Mater.* **54-57**, 1497 (1986).
- [13] J. J. Ying, X. F. Wang, X. G. Luo, A. F. Wang, M. Zhang, Y. J. Yan, Z. J. Xiang, R. H. Liu, P. Cheng, G. J. Ye, and X. H. Chen, arXiv: 1012.5552 (unpublished).
- [14] W. Bao, Q. Huang, G. F. Chen, M. A. Green, D. M. Wang, J. B. He, X. Q. Wang, and Y. Qiu, arXiv: 1102.0830 (unpublished).
- [15] F. Ye, S. Chi, W. Bao, X. F. Wang, J. J. Ying, X. H. Chen, H. D. Wang, C. H. Dong, and M. H. Fang, arXiv: 1102.2882 (unpublished).
- [16] L. J. Zhang and D. J. Singh, *Phys. Rev. B* **79**, 094528 (2009).
- [17] P. Blaha, K. Schwarz, G. K. H. Madsen, D. Kvasnicka, J. Luitz, WIEN2k, An Augmented Plane Wave Plus Local Orbitals Program for Calculating Crystal Properties, Vienna University of Technology, Vienna, Austria, 2001.

- [18] S. Graser, A. F. Kemper, T. A. Maier, H. P. Cheng, P. J. Hirschfeld, and D. J. Scalapino, Phys. Rev. B **81**, 214503 (2010).
- [19] K. Kubo, Phys. Rev. B **75**, 224509 (2007).
- [20] S. Graser, T. A. Maier, P. J. Hirschfeld, and D. J. Scalapino, New Journal of Physics **11**, 025016 (2009).
- [21] M. H. Fang, H. D. Wang, C. H. Dong, Z. J. Li, C. M. Feng, J. Chen, and H. Q. Yuan, arXiv: 1012.5236 (unpublished).
- [22] X. W. Yan, M. Gao, Z. Y. Lu, and T. Xiang, arXiv: 1102.2215 (unpublished).
- [23] X. W. Yan, M. Gao, Z. Y. Lu, and T. Xiang, Phys. Rev. Lett. **106**, 087005 (2011).